Received: 14 March 2022 | Accepted: 12 July 2022

DOI: 10.1111/gcb.16397

Global Change Biology WILEY

RESEARCH ARTICLE

Emergence of the physiological effects of elevated CO_2 on land–atmosphere exchange of carbon and water

Chunhui Zhan[1] | René Orth[1] | Mirco Migliavacca[1,2] | Sönke Zaehle[3] | Markus Reichstein[1] | Jan Engel[3] | Anja Rammig[4] | Alexander J. Winkler[1]

[1]Department for Biogeochemical Integration, Max Planck Institute for Biogeochemistry, Jena, Germany

[2]European Commission, Joint Research Centre, Ispra, Italy

[3]Department of Biogeochemical Signals, Max Planck Institute for Biogeochemistry, Jena, Germany

[4]Land Surface-Atmosphere Interactions, TUM School of Life Sciences Weihenstephan, Technical University of Munich, Freising, Germany

Correspondence
Chunhui Zhan, Department for Biogeochemical Integration, Max Planck Institute for Biogeochemistry, Jena, Germany.
Email: czhan@bgc-jena.mpg.de

Funding information
German Research Foundation, Grant/Award Number: 391059971; H2020 European Research Council, Grant/Award Number: 647204 and 855187; International Max Planck Research School for Global Biogeochemical Cycles

Abstract

Elevated atmospheric CO_2 (eCO_2) influences the carbon assimilation rate and stomatal conductance of plants, thereby affecting the global cycles of carbon and water. Yet, the detection of these physiological effects of eCO_2 in observational data remains challenging, because natural variations and confounding factors (e.g., warming) can overshadow the eCO_2 effects in observational data of real-world ecosystems. In this study, we aim at developing a method to detect the emergence of the physiological CO_2 effects on various variables related to carbon and water fluxes. We mimic the observational setting in ecosystems using a comprehensive process-based land surface model QUINCY to simulate the leaf-level effects of increasing atmospheric CO_2 concentrations and their century-long propagation through the terrestrial carbon and water cycles across different climate regimes and biomes. We then develop a statistical method based on the signal-to-noise ratio to detect the emergence of the eCO_2 effects. The eCO_2 effect on gross primary productivity (GPP) emerges at relatively low CO_2 increase ($\Delta[CO_2] \sim 20$ ppm) where the leaf area index is relatively high. Compared to GPP, the eCO_2 effect causing reduced transpiration water flux (normalized to leaf area) emerges only at relatively high CO_2 increase ($\Delta[CO_2] >> 40$ ppm), due to the high sensitivity to climate variability and thus lower signal-to-noise ratio. In general, the response to eCO_2 is detectable earlier for variables related to the carbon cycle than the water cycle, when plant productivity is not limited by climatic constraints, and stronger in forest-dominated rather than in grass-dominated ecosystems. Our results provide a step toward when and where we expect to detect physiological CO_2 effects in in-situ flux measurements, how to detect them and encourage future efforts to improve the understanding and quantification of these effects in observations of terrestrial carbon and water dynamics.

KEYWORDS
carbon cycle, CO_2 fertilization, hyrdological cycle, land-atmosphere interactions, signal detection, terrestrial biosphere and Earth system model, terrestrial ecosystems

1 | INTRODUCTION

Plants are tightly coupled to the ambient atmosphere through their exchange of energy, water, and carbon. Through this coupling, plants play an essential role in controlling the global cycles of carbon and water, and also modulate earth's surface energy balance (Denissen et al., 2022; Friedlingstein et al., 2019; Gedney et al., 2006; Williams & Torn, 2015). Changing atmospheric conditions such as rising air temperature, or increasing dryness in turn directly impact on plants and their functioning (Bastos et al., 2020; Novick et al., 2016; Reichstein et al., 2013). Also changes in the atmospheric composition, such as elevated atmospheric CO_2 (eCO_2), alter plant productivity, for example by stimulating carbon assimilation and by reducing stomatal conductance (Ainsworth & Long, 2005; Norby & Zak, 2011; Walker et al., 2021). As a result, the light-use efficiency (LUE; Drake et al., 1997) and the water-use efficiency (WUE) of plants (WUE; Peñuelas et al., 2011; Ueyama et al., 2020) increase under eCO_2. The combined effect is referred to as the CO_2 fertilization effect (Körner et al., 2007; Walker et al., 2021). This study aims to identify the change in atmospheric CO_2 concentrations at which the eCO_2 effects are distinguishable from the short-term and long-term climate effects.

Plant leaves respond directly to eCO_2 through the physiological mechanisms associated with the CO_2 fertilization effect, which could potentially translate into changes in gross primary productivity (GPP) and transpiration (Tr) that can propagate further into the carbon and water cycles (Fernández-Martínez et al., 2017; Lemordant et al., 2018; Walker et al., 2021). Throughout this paper, the eCO_2 effects indicate particularly physiological effects. Specifically, the eCO_2 effect alters the carbon cycle by triggering changes in GPP resulting in changes in net primary production (NPP) and various aspects of biomass production, accumulation, and allocation (e.g., leaves or roots). The increased biomass production can potentially contribute to an increased leaf area index (LAI). Observational evidence suggests that this effect can vary substantially across different biomes and plant functional types (De Kauwe et al., 2014; Norby & Zak, 2011; Winkler et al., 2021). The water cycle is affected as eCO_2 is triggering changes in the leaf-level Tr flux which controls the largest fraction of the land–atmosphere water exchange (Good et al., 2015). The eCO_2-induced change of Tr implies a potential influence on other components in the water cycle, such as soil evaporation, run-off, and consequently soil moisture (Lemordant et al., 2018; Leuzinger & Körner, 2007). However, reduced transpiration at the leaf level due to reduced stomatal conductance and stomatal density in response to eCO_2 (Ainsworth & Rogers, 2007; Woodward & Kelly, 1995) could be offset by a simultaneous increase in leaf area, and thus transpiration at canopy level as more carbon is invested in leaf growth in response to eCO_2 (Wullschleger et al., 2002). These competing effects of eCO_2 could potentially compensate each other, resulting in a non-detectable effect on the water cycle. On the other hand, the increasing leaf area enhances GPP by controlling light interception (McCarthy et al., 2006).

The emergence of the effects of eCO_2 on carbon and water cycles in experiments and observations remain inconsistent. The intrinsic WUE inferred from 21 flux site measurements shows strong increase (Keenan et al., 2013), while the study by Knauer et al. (2017) indicates a smaller magnitude of WUE response at a recent large scale. Increased biomass is found in many free-air CO_2 enrichment (FACE) experiments (Walker et al., 2019). However, tree-ring studies indicate the increased intrinsic WUE does not translate into the increased tree biomass (Peñuelas et al., 2011; van der Sleen et al., 2015). The diverse response of plant physiology to eCO_2 is observed in many other aspects. Results from field experiments show the magnitude of eCO_2 stimulation on carbon assimilation rate varies considerably across species and experimental conditions (Leakey et al., 2009; Norby et al., 1999; Norby & Zak, 2011; Walker et al., 2021). Meta-analysis indicates that stomatal conductance in young trees shows stronger response to eCO_2 than old trees, and deciduous forest shows stronger response than conifer forest (Medlyn et al., 2001). Furthermore, photosynthesis in C4 plants is close to being saturated, while plants in the C3 carbon pathway are expected to show a greater increase in carbon assimilation rate (Ainsworth & Rogers, 2007; Kramer, 1981; Leakey et al., 2009). C4 plants may have more potential response to eCO_2 associated with high WUE (Way et al., 2014). Overall, the uncertain strength of eCO_2 effects across different climate zones and biomes prevents us from better understanding the governing processes, but this is necessary to anticipate future changes of carbon and water fluxes in the system.

This study aims to develop a methodology that would be helpful to define the detectable imprint of CO_2 on land–atmosphere fluxes of carbon and water given the natural variabilities. Such a detection is challenging with real-world data, mostly due to confounding factors impacting on long-term plant productivity, such as climatic variability, nitrogen deposition, and land cover change (Fernández-Martínez et al., 2017; Liu et al., 2021; McCarthy et al., 2010; Schimel et al., 2015). FACE experiments provide the opportunities to observe the response of ecosystems to eCO_2 in the field exposed in open-air conditions (Ainsworth & Long, 2005). Nevertheless, in these experiments, ecosystems are pushed into an "accelerating mode" where plants are exposed to a much higher rate of CO_2 concentration increase (≈550 ppm) in a short time period while the climate conditions are changing at a relatively slow speed. Process-based models provide the opportunity to conduct factorial experiments to isolate the role of individual drivers, which allows us to test a statistical trend-detection method. Using this method, we develop the concept of the emergence of the eCO_2 effect (EoC), which allows us to determine to which extent the eCO_2 effect can exceed the natural variability and confounding factors. Here, we perform three simulations with the terrestrial biosphere model QUINCY (QUantifying Interactions between terrestrial Nutrient CYcles and the climate system; Thum et al., 2019) to isolate the eCO_2 effects: (i) a reference simulation with transient CO_2 concentrations and observation-based meteorological forcing, (ii) a simulation where the CO_2 is kept

constant at the level of 1901 while the meteorological forcing is identical to the reference simulation; and (iii) a simulation with the same set up of (i) but CO_2 is kept constant after the year 1988 at the level of 1988. The simulation (iii) is used to test our method in the recent time period, when the FLUXNET observations start to be recorded (Baldocchi et al., 2001). Additionally, the simulation (iii) is designed to study the role of the baseline CO_2 concentration in our findings. Analyzing the differences of carbon and water fluxes between simulations with transient and constant CO_2 concentration, we develop a statistical method based on the signal-to-noise ratio to detect the emergence of significant eCO_2 effects on these fluxes given their natural variability. The signal refers to the eCO_2 effects, and the noise indicates the inter-annual variability which is related mostly to climate variations. In other words, we seek to identify the point in time when the signal is distinguishable from the noise. We concentrate on the two variables which are most directly affected by rising CO_2, GPP, and Tr at annual, seasonal, and diurnal scales. To exclude the potential compensation effect of increasing LAI, we normalize Tr by LAI (Tr_{norm}) to obtain the transpiration flux per leaf area. Subsequently, we analyze eCO_2 effects on ecosystem properties (Table 1) which are important in the carbon and water cycle and investigate controls of the EoC. We also include Earth system models (ESMs) from the most recent Coupled Model Intercomparison Project (CMIP6) to examine the controls of the EoC in other models than QUINCY with different process formulations. In this way, we validate to which extent the controls of spatial variations in EoC found from QUINCY also apply for CMIP6 simulations. Overall, this analysis will guide the investigation of the eCO_2 effects in measurements of water and carbon fluxes as being conducted at the various eddy covariance sites.

TABLE 1 Variables and metrics analyzed for the emergence of the elevated CO_2 effects

Variable or metric	Abbreviation
Gross primary productivity	GPP
Transpiration	Tr
Normalized transpiration per leaf area (*Tr / LAI*)	Tr_{norm}
Leaf area index	LAI
Net primary production	NPP
Biomass	
Evaporation	
Interception loss	
Root-zone soil moisture	
Light-use efficiency (*GPP/Absorbed photosynthetically active radiation (APAR)*)	LUE
Underlying water-use efficiency ($GPP \times \sqrt{VPD} / Tr$)	uWUE
Normalized canopy conductance (*canopy conductance (gc)/(VPD × LAI)*)	gc_{norm}
95th percentile of daily GPP values in each year	GPP^{95}
95th percentile of daily Tr_{norm} values in each year	Tr_{norm}^{95}

2 | MATERIALS AND METHODS

2.1 | QUINCY model

2.1.1 | Model description

The terrestrial ecosystem model, QUINCY (Thum et al., 2019), is designed to represent the coupled carbon, nitrogen, and phosphorus cycles and their interactions with energy and water balances in terrestrial ecosystems. QUINCY simulates half-hourly carbon, water and energy fluxes as well as longer-term ecosystem dynamics across climate regimes and different plant functional types (PFTs), representing different plant growth forms (tree, grass), leaf types (leaves, needles), and phenology (evergreen, cold and drought deciduous, perennial). Calculation of coupled photosynthesis (Kull & Kruijt, 1998) and stomatal conductance (Medlyn et al., 2011) are taking for sunlit and shaded leaves separately along the vertical canopy gradient of light, foliar chlorophyll, and photosynthetic N. QUINCY accounts for limitations of photosynthesis by light, CO_2, temperature, and water availability. Light attenuates in the canopy with exponentially increasing layer thickness when the canopy depth increases as a function of the cumulative LAI. GPP at the canopy level is integrated from leaf-level gross photosynthesis. The simulated diurnal and seasonal patterns of GPP have been evaluated against a number of benchmarks, including several FLUXNET sites. Leaf area development is dynamically dependent on plant production (and thereby its response to changing atmospheric CO_2, climate and water availability) as well as stand structural development and turnover through mortality and establishment. Transpiration is calculated as a function of the stomatal conductance of the canopy, aerodynamic conductance, and other parameters in terms of air density and humidity. Soil physics, moisture, and biogeochemistry are modelled for 15 layers with exponentially increasing depth. QUINCY calculates the litter and soil organic matter turnover by first-order kinetics with temperature and moisture dependencies. For more detailed explanations of the process representations in QUINCY, please refer to the model description by Thum et al. (2019). The code version used in this study (see code availability statement) corresponds to that of Thum et al. (2019), with minor bug fixes affecting the stability of the energy balance calculation, the calculation of grassland phenology as well as the use of the stomatal model by Medlyn et al. (2011).

2.1.2 | Model setup

Boundary conditions and meteorological forcing

The QUINCY model is a 1D model applied at individual sites (336 sites) distributed across climate zones and biomes for the time period 1901–2018. As an offline land surface model, QUINCY takes time-dependent observation-based meteorological forcing variables as input such as short- and longwave radiation, air temperature, precipitation, vapor pressure deficit (VPD), atmospheric CO_2 concentration, as well as other boundary conditions such as

geographic coordinates, PFTs, and soil physical and chemical parameters. At each site, a specific boundary condition and meteorological forcing are taken from the Climate Research Unit and Japanese reanalysis product (CRU JRA V2.1; Harris et al., 2020), and disaggregated to the model time step (half-hourly) using the statistical weather generator (Zaehle & Friend, 2010). The annual atmospheric CO_2 concentration is obtained from the Global Carbon Project (Le Quéré et al., 2018). Soil physical and chemical properties are derived from soil texture (Saxton & Rawls, 2006). The texture data are taken from the nearest grid cell of SoilGrids dataset (Hengl et al., 2017). To improve the interpretability of the model simulations with respect to the occurrence of the eCO_2 signal, we reduce the model complexity and set the soil-soluble NH_4, NO_3, and PO_4 concentrations at a prescribed level so that the plant growth is not limited by the nutrient availability, and disregard the N and P deposition in the model.

Model simulation experiments for hypothesis testing

We conduct three factorial model experiments to disentangle the effects of eCO_2 from other drivers: (a) transient-CO_2 experiment. This simulation can be considered as a historical run that aims to approximate the observed system and thus takes the transient climate and CO_2 concentration for the period 1901–2018 as forcing. The transient-CO_2 experiment simulates an increase in atmospheric CO_2 of 110.63 ppm over 118 years; (b) constant-CO_2 experiment. This simulation includes the same transient climate as the transient-CO_2 experiment. However, the atmospheric CO_2 concentration does not change and is fixed to the initial value of 1901 (296.8 ppm) for the entire simulation period. The climate forcing data contain the effects of rising CO_2. (c) freeze-CO_2 experiment. Here, the atmospheric CO_2 increases until 1988, as in the transient-CO_2 experiment, but is then kept constant at this value in the years thereafter. The year 1988 was chosen as the time close to the setup of the first FLUXNET sites (Baldocchi et al., 2001).

2.2 | Statistical analysis

2.2.1 | The effect of elevated CO_2 on annual average GPP and Tr_{norm}

We first calculate the difference in annual average values of GPP and normalized transpiration (Tr_{norm} = Tr/LAI) between the transient-CO_2 and the constant-CO_2 experiments. The difference indicates the eCO_2 effect on the target variable for the period 1901–2018. We cluster the sites based on site-PFT in four vegetation groups: tropical forest, temperate forest, boreal forest, and grasses (Table S1). We further classify the sites of each vegetation group into three temperature classes, "hot," "warm," and "cold" based on the quantiles of long-term mean 2 m air temperature between the sites in each group. Subdividing the temperature classes further based on the long-term mean annual precipitation ("low," "middle," and "high"), we are able to assess the role of water availability in controlling the variability in GPP and normalized transpiration. While the CO_2-induced change of LAI compensates the reduced leaf-level water loss at canopy Tr, it governs GPP in an opposite way. The structural change of increased LAI increases the amount of absorbed photosynthetically active radiation (APAR) and therefore vegetation productivity. We also evaluate the eCO_2 effect on annual average LUE (LUE = GPP/APAR). The part of increased GPP related to increased LAI can be thus disentangled.

2.2.2 | Emergence of the elevated CO_2 effects

Based on the CO_2 fertilization effect, we hypothesize that the continuous CO_2 increase over a long period of time exerts a significant influence on the ecosystem (e.g., GPP), which stands out as the eCO_2 effect from natural variability and other factors after a given time and strength of atmospheric CO_2 concentration increase. We define the EoC (ppm) as the change in CO_2 concentration ($\Delta[CO_2]$) required so that the annual mean values of a simulated variable in the transient-CO_2 experiment diverges significantly from the constant-CO_2 experiment. The significant divergence between the annual mean values is defined by the point in $\Delta[CO_2]$ when the signal exceeds the noise. The noise is intended as the interannual variability of the signal around the long-term changes. We retrieve the signal and noise from the linear fit in the historical time period for each experiment. The calculation of EoC consists of four steps: (1) for each site, we calculate annual averages for the target variable (e.g., GPP) from daily model output for both transient-CO_2 and constant-CO_2 experiments for the time period 1901–2018. We calculate the absolute increase of the annual mean CO_2 level (i.e., $\Delta[CO_2]$) compared with the CO_2 concentration in the initial year in the transient-CO_2 experiment; (2) we apply linear least squares regressions to retrieve the trend in the evolution of the target variable along $\Delta[CO_2]$ from both transient- and constant-CO_2 experiments, respectively, over a given time period (Figure 1). We start with the time period 1901–1910 and iteratively expand this time period year by year by advancing the final year of the time window. For each time period, we compute the linear trend between the target variable and the $\Delta[CO_2]$ and the uncertainty of the estimation. Accordingly, we obtain an estimate of the trend and its uncertainties for a total of $n = 108$ points in time for each experiment at each site. The trend b and its standard error $\sigma_b$in the linear regression model are given by (Weisstein, n.d.):

$$b = \frac{\sum_{i=1}^{n}(x_i-\overline{x})(y_i-\overline{y})}{\sum_{i=1}^{n}(x_i-\overline{x})^2}$$

$$\sigma_b = \sqrt{\frac{\left(\sum_{i=1}^{n}(y_i-\overline{y})^2-\left(\sum_{i=1}^{n}(x_i-\overline{x})(y_i-\overline{y})\times b\right)/(n-2)}{\sum_{i=1}^{n}(x_i-\overline{x})^2}}$$

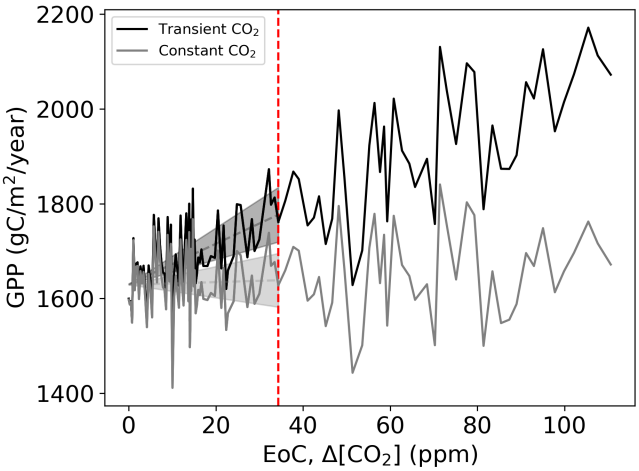

FIGURE 1 Illustration of detection of emergence of the elevated CO_2 effects (EoC). The solid lines depict the evolution of annual mean gross primary productivity (GPP) along increasing CO_2 levels for one example site in QUINCY (80.75°W, 37.75°N, temperate broadleaved summer green tree). Black color denotes the evolution of GPP from the transient-CO_2 experiment, while gray color denotes the evolution of GPP from the constant-CO_2 experiment (for details, see Section 2.1.2.2), in which CO_2 is used as the proxy of time. The shaded area represents the standard error of the linear regression slope (black or gray dashed line). The vertical dashed red line indicates the EoC, that is, the value of Δ[CO_2] where the black and gray trends deviate significantly.

where x is the Δ[CO_2] at time step i, and y is the value of target variable at time step i; (3) the signal is retrieved as the absolute difference in the regression slopes Δb (b in transient-CO_2 minus b in constant-CO_2) as a function of Δ[CO_2], while the noise is estimated based on twice the sum of two σ_b from the transient-CO_2 and constant-CO_2 experiments to represent the statistical significance (two-sigma rule); (4) the EoC is defined as CO_2 concentration difference (Δ[CO_2]) between the time when the signal exceeds the noise for 5 consecutive years for the first time and the year 1901 (see Figure 1 for example). We also test the sensitivity of the arbitrary choice of 5 years in the calculation of EoC and present results also for n (n = 3, 5, 7, 9) years (Figure S4). We show that the impact of our arbitrary choice is negligible on the results. Even though there could be a meteorological extreme event that has a strong impact in individual years, it has a limited influence on the slope of the linear regression over many years. For analyzing the freeze-CO_2 experiment, we use the same approach to derive the EoC. The only difference is that we set the initial year of keeping CO_2 constant to 1988 instead of 1901.

This freeze-CO_2 approach makes sure that both experiments (transient and freeze-CO_2) share the same initial state and memory in the system. In addition and comparison to the freeze-CO_2 experiment, we assess this aspect also using the transient and constant-CO_2 experiments and derive the sensitivity of EoC over time by advancing the initial year (i.e., 1901, 1930, 1960, and 1988) in the analysis. In doing so, we shift the time series of the dependent variable (e.g., GPP) in the constant-CO_2 experiment along the y-axis to match the value in the transient-CO_2 experiment in the respective initial year. In this analysis, we calculate EoC with varying initial states (Figure S13).

In this study, we mainly focus on the CO_2-induced change on annual average values of the relevant variables and metrics for all sites. Based on existing knowledge, we select variables or metrics (Table 1) that are hypothesized to be most sensitive to eCO_2 (Drake et al., 1997; Knauer et al., 2017; Migliavacca et al., 2021; Novick et al., 2016; Ueyama et al., 2020) to investigate the first manifestations of eCO_2. In addition, to analyze the variation of the CO_2 fertilization effect at different time scales, we apply the same detecting method at specific times-of-day in each year (e.g., 1 May, 8 am) instead of annual means, to derive the EoC at seasonal and diurnal scales for representative sites from each vegetation classes (Table S1).

Next to this trend-detection method, an alternative method is implemented to test the robustness of the current method. The alternative method defines the signal as the mean of the difference between the time series of the target variable from the transient- and constant-CO_2 experiments. The noise is estimated using twice the sum of the standard error in residuals from both time series after removing the long-term trend using the LOWESS fit function (Cleveland, 1981). The time of emergence is determined by the year when the signal exceeds the noise for 5 consecutive years for the first time. The EoC is defined as the CO_2 concentration difference (Δ[CO_2]) between the time of emergence and the year 1901 (Figure S14).

2.2.3 | Variable importance determined with random forest analysis

After determining EoC for each site-level simulation, we obtain the respective spatial distribution of EoC across sites. We evaluate the relative contribution from all drivers to the spatial variability in EoC by applying SHapley Additive exPlanation (SHAP) value analysis based on the random forest (RF) model. First, we train the RF model (scikit-learn RandomForestRegressor API in Python; Pedregosa et al., 2011) to predict the previously computed EoC patterns across sites using site-specific long-term (1901–2018) means of climate factors (i.e., temperature, precipitation, soil moisture, VPD, aridity index [evapotranspiration/precipitation]) and vegetation related factors (i.e., GPP, LAI, growing season length) as predictors (Figure S10). The long-term mean values are computed over the entire simulation period from the transient-CO_2 experiment. The out-of-bag score estimates the accuracy of the prediction from the RF model as compared with the actual EoC values, where a higher value (the maximum score equals 1) represents a better performance of the model. Finally, we use the module "SHAP TreeExplainer" from the software package shap in Python (Lundberg et al., 2020; Lundberg & Lee, 2017) to examine the influence of all the involved predictors. The average of the absolute SHAP values for each predictor indicates its impact on the target variable (i.e., spatial variability of EoC).

2.3 | Comparison with simulations from ESMs (CMIP6)

In addition, we perform the EoC analysis for GPP and Tr_{norm} using simulations from 7 ESMs from the most recent CMIP6. We use simulation output of the CMIP6 experiments 1pctCO2 and 1pctCO2-rad. In both experiments, the CO_2 concentration increases gradually at a rate of 1% per year until quadrupling, starting at the pre-industrial equilibrium state (Meehl et al., 2014). The fully coupled model setup is used in the 1pctCO2 experiment, while for the 1pctCO2-rad experiment the CO_2 concentration is kept at the pre-industrial level for the carbon cycle and the increasing CO_2 has only a radiative effect (i.e., CO_2-induced climatic changes; Jones et al., 2016). Therefore, the 1pctCO2 experiment is comparable to our transient-CO_2 experiment, and the 1pctCO2-rad experiment is comparable to our constant-CO_2 experiment, although the QUINCY simulations follow the observed CO_2 concentration for the last 120 years. EoC is calculated by applying the same detection method as described in Section 2.2.2. To obtain comparability to the EoC results based on the QUINCY simulations, we select cells in gridded CMIP6 output which correspond to the locations of simulated sites with QUINCY. Furthermore, we only consider the CMIP6 time series from the year 1850 until the doubling of the atmospheric CO_2 concentration, that is, roughly 560 ppm. The ESMs used in this study are (1) Beijing Climate Center (BCC) BCC-CSM2-MR, (2) Institut Pierre Simon Laplace (IPSL) IPSL-CM6A-LR, (3) Centre National de Recherches Météorologiques (CNRM) CNRM-ESM2-1, (4) United Kingdom (UK) UKESM1-0-LL, (5) Canadian Centre for Climate Modelling and Analysis (CCCma) CanESM5, (6) Meteorological Research Institute of the Japan Meteorological Agency (MRI) MRI-ESM2-0, and (7) Max Planck Institute for Meteorology (MPI) MPI-ESM1.2-LR. More details on the used CMIP6 ESMs can be found in Arora et al. (2020). Due to missing respective output, the analysis for normalized transpiration (Tr_{norm}) only involves the first four models in the CMIP6 archive.

3 | RESULTS AND DISCUSSION

3.1 | The effect of elevated CO_2 on GPP

Our analysis based on model simulation experiments indicates that eCO_2 generally increases GPP. This increase in GPP differs in magnitude and interannual variability across climate and vegetation types (Figure 2). The trend of increasing GPP over 118 years is clearly visible in all forested sites and less clear at grassland sites due to high year-to-year variability in GPP. In comparison to the forested sites, the variability in GPP is considerably higher at grassland sites, because grass-dominated ecosystems are more sensitive to climate variability partly related to shallower roots (Kulmatiski et al., 2020; Miguez-Macho & Fan, 2021) and less regulated by stomatal closure (Konings et al., 2017). Grasslands are also predominantly located in semi-arid regions, in which interannual variability of precipitation is large, and therefore has a larger imprint on GPP that it would have in mesic ecosystems with lower precipitation interannual variability (Maurer et al., 2020). The grassland sites that are located in relatively cold regions show less variability and more clear trends in GPP in contrast to grassland sites located in warmer (and drier) regions.

Overall, the results show that the CO_2 fertilization effect is strong where vegetation productivity is not strongly limited by energy or water availability. Subdividing the temperature classes further based on the amount of annual precipitation, we are able to assess the role of water availability in controlling the variability in GPP (Figure S2). Sites located in relatively warm and wet regions in the temperate and the boreal forest vegetation class (Figure S2b,c) also exhibit the sharpest increase in GPP. This is probably related to the temperature-dependent response of photosynthetic rate of CO_2 uptake through the kinetics of the Rubisco enzyme (Baig et al., 2015; Hickler et al., 2008; Long, 1991). However, the difference of increase in LUE across temperature and precipitation classes is not apparent compared to where we

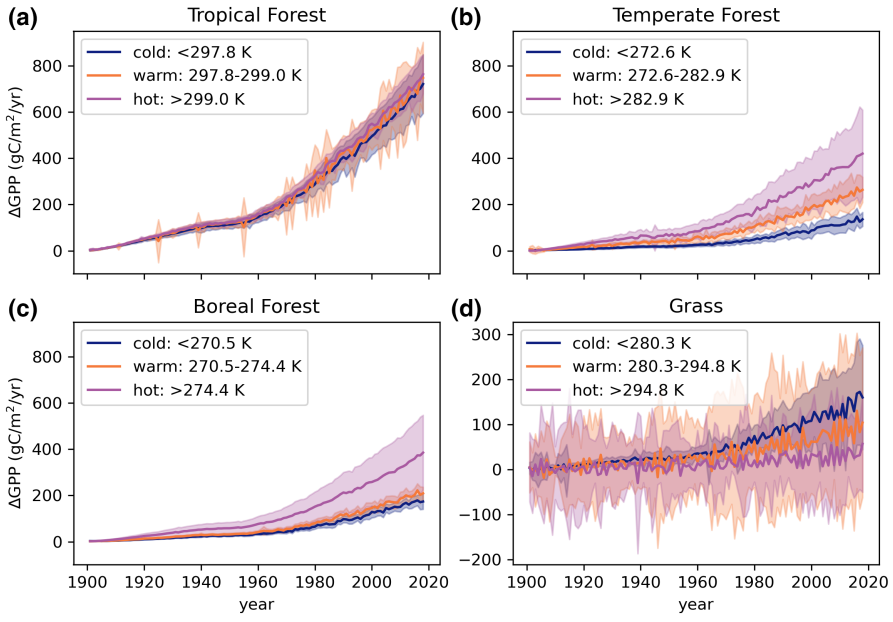

FIGURE 2 Differences in annual average gross primary productivity (GPP) between the transient-CO_2 and the constant-CO_2 experiments across climate and vegetation classes. All global sites (336 sites) are first grouped by vegetation type (a–d, Table S1) and then by long-term mean temperature using quantiles within each group (cold in blue: ≤0.33; warm in orange: 0.33–0.66; hot in purple: ≥0.66). The shaded area depicts standard deviation around the multi-sites mean value (solid lines).

find the sharp increase in GPP, especially in the temperate forest vegetation class (Figure S1). The increased carbon assimilation due to rising CO_2 leads to a build-up of more biomass, some of which is allocated to increased leaf growth resulting in an extension of the leaf area (Winkler et al., 2021). Canopies with higher LAI are more available for light interception and therefore it leads to enhancement of vegetation productivity. In temperate forest, the enhancement of GPP due to eCO_2 is the combination of increased both LAI and photosynthetic efficiency (McCarthy et al., 2006; Norby et al., 2005).

3.2 | The effect of elevated CO_2 on transpiration per leaf area

Decreased transpiration (Tr) due to down-regulated gas exchange with the atmosphere at the leaf level can be offset by an extension in leaf area at the canopy level. The simulated Tr exhibits both increasing and decreasing trends in response to eCO_2. To account for that, we normalized Tr by LAI which is denoted by Tr_{norm}. Tr_{norm} thus represents the transpiration per leaf area.

As expected, we find consistently decreasing Tr_{norm} across all vegetation types and temperature classes (Figure 3). Similar to the result in Section 3.1 (Figure 2), the variability in Tr_{norm} is high in grasslands. In contrast to GPP, Tr_{norm} responds to eCO_2 strongly where temperature and precipitation are relatively low (i.e., cold and try regions) except for tropical forest sites (Figure S3). Barton et al. (2012) suggested that the ratio of net photosynthesis to transpiration increases in proportion to the increase in atmospheric CO_2 concentration. They further demonstrated that stomatal conductance responds to eCO_2 not as strongly as the photosynthesis apparatus. At the leaf level, the decreased stomatal conductance is likely to result in the increase of leaf skin temperature (Leakey et al., 2009), which demands higher transpiration. However, the direct relationship between ambient temperature and eCO_2 effect on stomatal regulation is still ambiguous (Barton et al., 2012; Medlyn et al., 2001).

3.3 | Emergence of the elevated CO_2 effects (EoC) in GPP and Tr_{norm}

A lower EoC indicates a detection of eCO_2 effects earlier in the analyzed time period and thus a stronger response in the target variable to the eCO_2 effects compared to its background or natural variability. Our results show that the eCO_2 effect in GPP is strongest in the tropical forests. In total, 34 in 174 detected sites exhibit an EoC of less than 20 ppm (Figure 4). This means that a change in atmospheric CO_2 of 20 ppm is sufficient to detect the CO_2 fertilization effect in the GPP time series for those sites. The forested northern mid- and high latitudes also exhibit significant changes in GPP, which, however, is only detectable at much higher $\Delta[CO_2]$ (consistent with Schimel et al., 2015). GPP in arid regions is highly variable due to the high sensitivity toward intermittent water availability, and this prevents a detection of the CO_2 fertilization effect. The effect of eCO_2 on GPP further rarely emerges in regions dominated by C4 grasses, most likely because they are less responsive to eCO_2 due to their different photosynthetic pathway (Leakey et al., 2009). Also, evidence from FACE experiments suggests that trees exhibit the greatest response to eCO_2 compared to C3 and C4 grasses (Ainsworth & Long, 2005). The magnitude of plants' responses to eCO_2 comes down to the variations of photosynthetic capacity, which is indicated by the maximum rate of RuBisCO carboxylase activity (Vc_{max}) and the maximum rate of photosynthetic electron transport (J_{max}; Long, 1991). We find a similar pattern of distribution for EoC in LUE (Figure S5) with EoC in GPP, which could support the physiological effect of eCO_2 on GPP rather than structural change, namely the change of LAI. The result from the alternative method (see Section 2.2.2) does not show apparent difference (Figure S14).

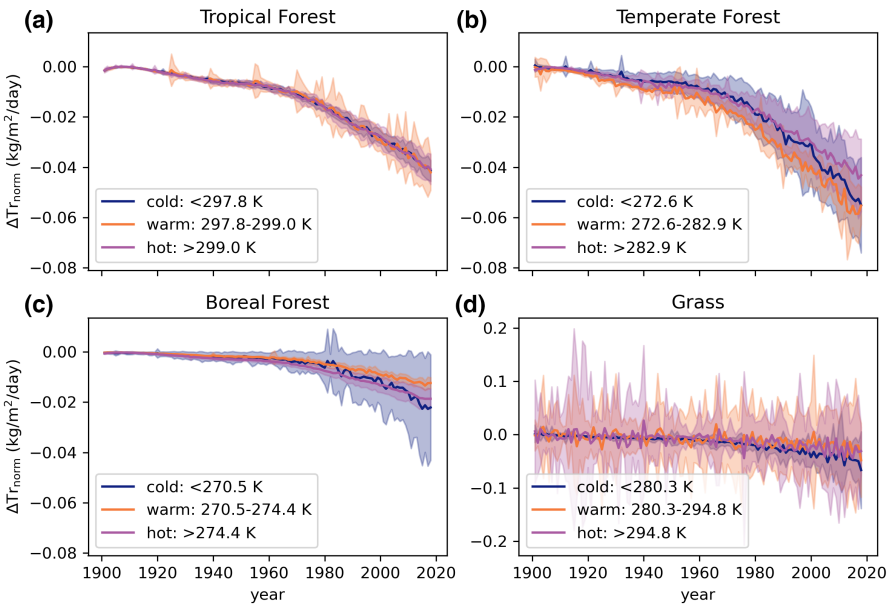

FIGURE 3 Differences in annual average Tr_{norm} between the transient-CO_2 and the constant-CO_2 experiments across climate and vegetation classes. All global sites (336 sites) are first grouped by vegetation type (a–d, Table S1) and then by temperature using quantiles (cold in blue: ≤0.33; warm in orange: 0.33–0.66; hot in purple: ≥0.66). The shaded area depicts standard deviation around the multi-sites mean value (solid lines).

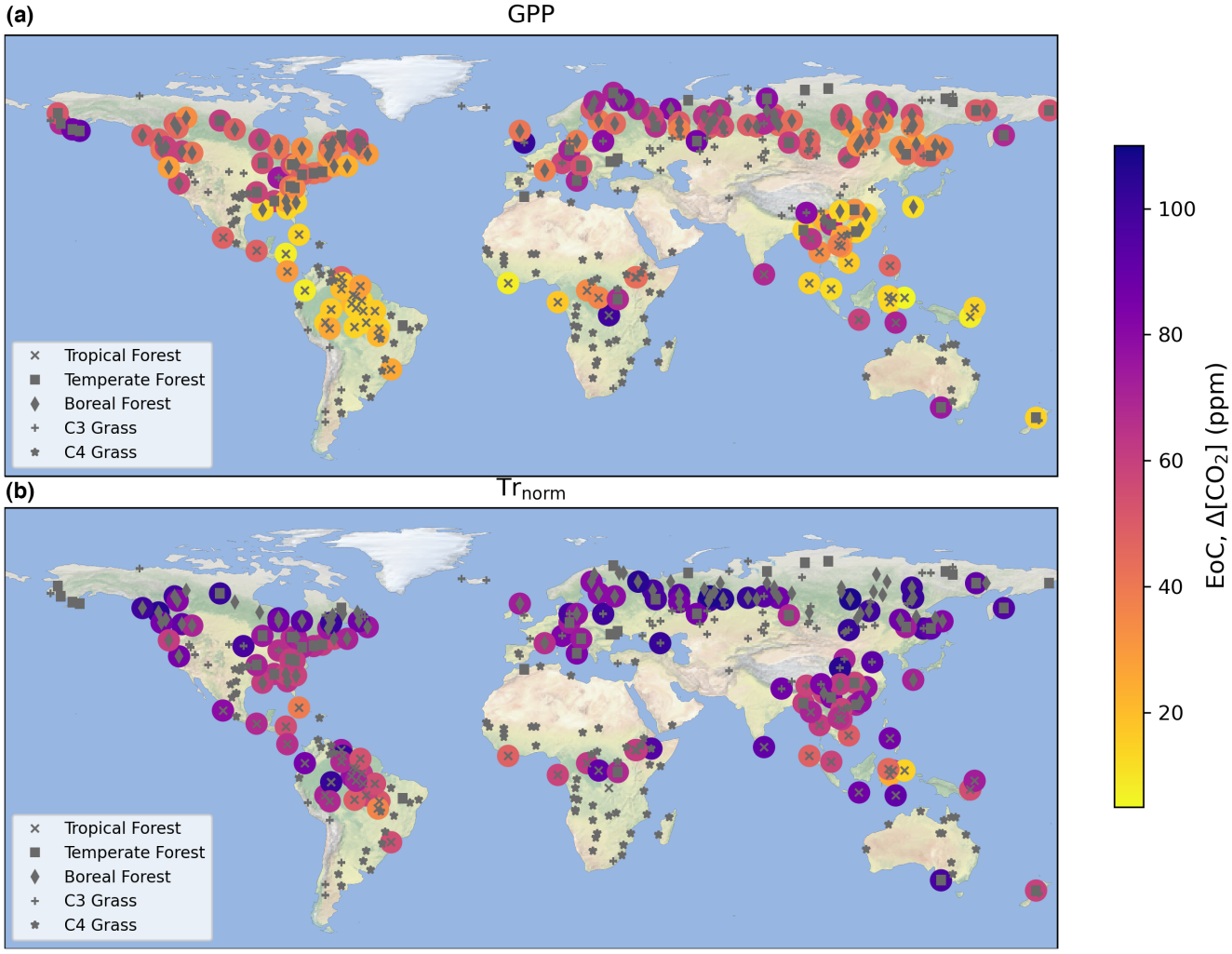

FIGURE 4 Spatial distribution of emergence of the elevated CO_2 effects (EoC) in (a) gross primary productivity (GPP) and (b) Tr_{norm}. Bright color indicates an earlier detection (lower EoC), and dark color indicates a later detection (higher EoC). Non-colored points indicate sites where the elevated CO_2 does not translate into significant changes in GPP or Tr_{norm} within the historical time period.

EoC in Tr_{norm} is substantially higher compared to GPP, that is, the signal emerges only at considerably higher $\Delta[CO_2]$. Furthermore, the global spatial pattern of EoC is more homogeneous for Tr_{norm} than for GPP. Several equatorial sites exhibit a relatively low EoC (some of them even less than 40 ppm), but for most sites (85 in 141 detected sites) the signal only emerges at $\Delta[CO_2] > 70$ ppm or not at all. Especially at sites in arid and semi-arid regions, no significant effect of eCO_2 can be detected, even though a strong response in WUE is expected to occur in these water-limited ecosystems (Medlyn et al., 2001). In the QUINCY model, canopy conductance and transpiration do not scale linearly with LAI at canopy level. So, the Tr_{norm} could still be affected by increasing LAI to some extent. Next to this, transpiration can be affected by other factors which may overshadow the role of stomatal conductance. For example, transpiration is affected by incoming radiation particularly when vegetation is strongly decoupled with the boundary layer, that is, a low exchange rate between vegetation and atmosphere (De Kauwe et al., 2017; Jarvis, 1985). Due to the limited representation of the coupling between vegetation and the boundary layer in models, the reduced transpiration flux at the leaf-level might not scale to the canopy-level.

The freeze-CO_2 experiment (see Section 2.1.2.2) reveals if the results are still informative for climate change in recent years (1988–2018). Due to the limited length of the time period, there are only a few sites where the eCO_2 effect on GPP can be detected (Figures S6 and S13). Nevertheless, as the result shown in Figure 4a, the signal first emerges in the tropical regions, with a rather low EoC of around 20 ppm. Furthermore, the EoC for tropical GPP is consistent between two time periods (1901–2018 and 1988–2018). This encourages future study of the CO_2 fertilization effect in recent years.

3.4 | Seasonal and diurnal variation of EoC in GPP

We find plants respond differently to the effects of eCO_2 across different climate zones and vegetation types, but also in different

seasons and times of the day. For example, EoC in GPP is lower in summer than in other seasons at sites in the temperate and boreal forests (Figure S7a,d), which is obviously driven by favorable growing conditions. However, this is not always the case at the diurnal time scale where lowest EoC are partly found at other times than noon. For the sites in temperate and boreal forests, the strong signal already emerges early in the morning on some days during summer. It could be related to the increased aridity at midday. The excessive atmospheric moisture demand at high temperature results in the midday depression of carbon uptake, and thus stomatal limitation, which can be simulated by the model. Unlike for the boreal forest site, at the tropical forest site (Figure S7b), the plant response to eCO_2 can be detected for any time during the daytime and in all seasons. Although the effect of eCO_2 on GPP cannot be detected at grass sites at the annual scale, we can detect it in the growing season, albeit only at very high $\Delta[CO_2] > \sim 100$ ppm (Figure 3, Figure S7c). The EoC in Tr_{norm} however is not detectable at any point of the seasonal and diurnal cycle, probably related to high variability of the meteorological conditions, which can be reduced to some extent by the aggregation to annual values. In the future, researchers may explore the drivers of the variation across diurnal and seasonal scales. Furthermore, we find the EoC in GPP is lower at some points of the seasonal and diurnal cycle than EoC in GPP at the annual scale (Figure S7). This motivates future study of eCO_2 effects in observations at the seasonal and diurnal time scale.

3.5 | EoC in secondary variables triggered by plant physiological effects

Changes in GPP and Tr_{norm} triggered by the effects of eCO_2 can cascade into secondary state and process variables of the carbon (e.g., LAI, biomass, NPP) and water cycles (e.g., evaporation, interception loss, soil moisture). The EoC in LAI and biomass are generally low (Figure S8a,b), even lower than in the case of GPP. Note that this does not mean that LAI responds more strongly to CO_2 increases than GPP, but rather this finding illustrates the effect of the internal variabilities of each variable on our results where LAI and biomass as state variables are less influenced by short-term and interannual hydro-meteorological variations and therefore its variation has a substantially lower standard deviation. The higher signal-to-noise ratio enables the detection of the eCO_2 effects already early in the time series where CO_2 has not yet increased much. Additionally, there is a non-linear relationship between GPP and LAI when LAI is high. GPP tends to saturate with high LAI due to clumping and the increase in shaded leaves in the canopy (Chen et al., 2012; Lee et al., 2019; Street et al., 2007). Furthermore, the modeled carbon pathways do not always agree with observational evidence from elevated CO_2 experiments (Norby & Zak, 2011). EoC in NPP shows a similar spatial pattern compared to EoC in GPP, only the EoC is overall higher due to the added variability from autotrophic respiration (Figure S8c). We note that vegetation in the natural ecosystem is limited by nutrient availability. The primary way, in which nutrient availability would interfere with the detectability method, is that there is less of a change in LAI compared to the change simulated assuming that nutrients were not limiting plant growth. For the development of the EoC method here, the complication of nutrient cycling in terrestrial biosphere models is equally unimportant as the question of ecosystem management. Thus, we simplify the setting in the model to pursue an understandable interpretation.

The natural variability of process and state variables in the water cycle (e.g., evaporation, interception, root-zone soil moisture) is substantially higher than for the carbon cycle variables. The increasing LAI could provide more shading area, resulting in a cooling of the surface soil layer. The evaporation from bare soil decreases as a consequence of this reduced radiative energy input. Consequently, the EoC in evaporation can be detected in sites located mainly in tropical regions and mid-latitude regions (Figure S8d). Evaporation from rainfall interception is expected to remarkably increase due to the substantial increase in LAI. However, the magnitude of increased interception loss does not stand out from the year-to-year variability controlled by stochastic precipitation events. Also, the root-zone soil moisture does not exhibit a clear response to eCO_2. This is related to the complex and interacting effects on related water fluxes such as soil evaporation, transpiration, interception loss, and runoff. The interannual variability in precipitation likely also overshadows the subtle changes in soil moisture in response to the effects of eCO_2 (De Kauwe et al., 2021).

3.6 | First manifestations of elevated CO_2

In this section, we compare the EoC across several variables and metrics (Table 1) related to the carbon and water cycles. These variables and metrics include the underlying WUE (uWUE), the LUE, the normalized canopy conductance (gc_{norm}), LAI and the 95th percentiles of GPP (GPP^{95}), and Tr_{norm} ($Tr_{norm}{}^{95}$). EoC is lowest for LAI and GPP^{95} for most sites (159 in 250 detected sites; Figure 5). We consider the 95th percentile of daily GPP values in each year (GPP^{95}) to be representative of the maximum capacity of vegetation productivity, which is less affected by day-to-day weather variability. EoC in GPP^{95} is significantly lower since much of the variability is removed compared to annual mean GPP. EoC in GPP^{95} and LAI are comparable in the vegetation classes tropical and boreal forests (Figure S9). However, EoC in LAI in the temperate forests and grass vegetation classes tends to be considerably higher. Probably, this is due to the different fraction of carbon allocated to foliage versus other plant components across vegetation types (De Kauwe et al., 2014).

EoC in LUE emerges first for sites located in the high latitudinal regions, where plant growth is considered to be energy limited. EoC in WUE and gc_{norm} emerges first for sites in arid regions, where plant growth is limited by water availability. Compared to variables related to the carbon cycle (e.g., GPP, GPP^{95}, LAI), variables related to the water cycle (e.g., gc_{norm}, Tr_{norm}, $Tr_{norm}{}^{95}$) show weaker responses to the physiological effects of eCO_2.

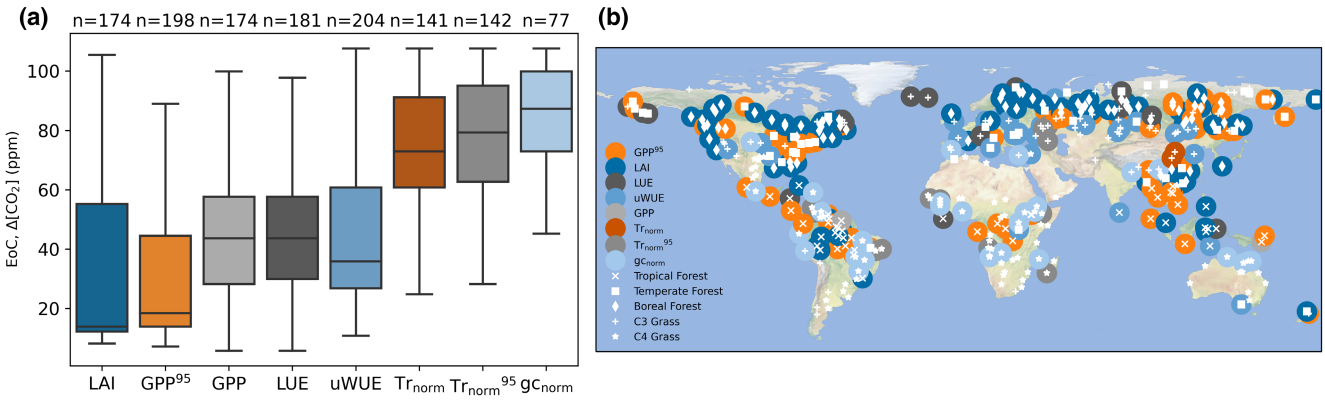

FIGURE 5 Comparison of EoC across variables and metrics. (a) Box plots depict the gross primary productivity (GPP), 95th percentile of daily GPP values in each year (GPP^{95}), leaf area index (LAI), light-use efficiency (LUE), underlying water-use efficiency (uWUE), gc_{norm}, Tr_{norm}, 95th percentile of daily Tr_{norm} values in each year (Tr_{norm}^{95}). Box plots indicate medians and interquantile ranges, and are ordered according to the mean EoC across sites for each variable. Numbers above the boxplots indicate how many sites can be detected for each variable or metric (336 sites in total). (b) The map shows the first-emerging variable or metric with the lowest EoC. The white points on the map refer to the geographical locations of all sites.

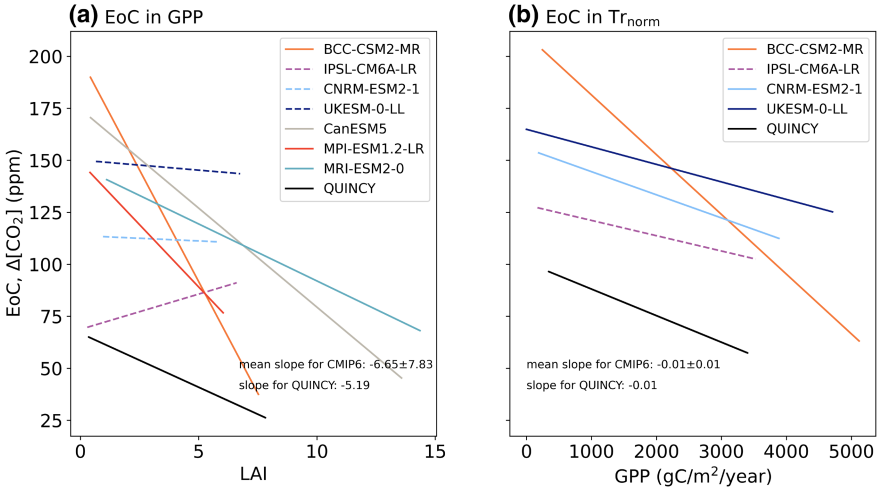

FIGURE 6 EoC in QUINCY versus coupled Earth system models (ESMs). Spatially varying EoC is plotted against the predictor that explains most of its spatial variability according to the SHAP value analysis illustrated in Figure S10. The relationship of (a) EoC in gross primary productivity (GPP) is plotted against respective leaf area index (LAI) of each model; and (b) EoC in Tr_{norm} is plotted against respective baseline GPP from each model. The dashed line denotes no significant relationship between EoC and the predictor.

3.7 | Explaining the spatial variability of EoC in GPP and Tr_{norm}

The ecosystem responses to eCO_2 are complex and modulated by several concurrent effects. All drivers considered to explain the spatial variability of EoC are calculated as long-term mean values (see Section 2.2.3). We find that the spatial variability of EoC in GPP and Tr_{norm} between sites is mainly explained by varying levels of mean LAI and mean GPP, respectively (Figure S10). The higher the mean LAI (or mean GPP), the less $\Delta[CO_2]$ is required such that the physiological effects of eCO_2 emerge in GPP, respectively, Tr_{norm} fluxes. Next, we compare these relationships based on the QUINCY model with output from similar simulations of Earth system models conducted in CMIP6 (see Section 2.3). Most CMIP6 models qualitatively agree with the QUINCY results, that is, the negative relationship between spatial EoC in GPP and LAI, and the negative relationship between spatial EoC in Tr_{norm} and GPP (Figure 6). Four models in CMIP6 (Figure S11a,e,f,g) agree with QUINCY (Figure S11h), while the other three of them do not show a negative relationship between EoC in GPP and the long-term mean LAI. Also, there are considerable differences between the magnitude of EoC across the models as well as the strength of the relationships vary among the individual models in CMIP6 (Figures S11 and S12). We note, however, that this direct comparison between the QUINCY and the CMIP6 simulations is limited due to the conceptually different setup of the analyzed simulations. Furthermore, in contrast to the QUINCY model, which is an offline terrestrial biosphere point model, the CMIP6 ensemble comprises fully coupled Earth system models, which represent a gridded and coupled land–atmosphere system. Despite these conceptual differences, the overall agreement between the QUINCY and CMIP6 models illustrated in Figure 6 corroborates our findings based on the QUINCY model formulation.

4 | CONCLUSION

We evaluate the plant physiological effects of elevated CO_2 (eCO_2) on the land–atmosphere exchange of carbon and water. Increasing

atmospheric CO_2 stimulates plant carbon assimilation and reduces stomatal conductance, which both may result in a potential increase in ecosystem productivity and also affect ecosystem transpiration. Analyzing approximately the last 120 years simulated by the terrestrial biosphere model QUINCY, we assess how strong the increase in CO_2 needs to be such that the effects of eCO_2 surpass the noise and effects induced by short and long-term meteorological conditions.

We find that the eCO_2 effects on GPP can be earlier detected compared with transpiration (Tr). The eCO_2 effects on GPP are different across climate and biomes, whereas eCO_2 effects on normalized transpiration (Tr_{norm}) exhibit less spatial variability. The eCO_2 effects on GPP are detectable at relatively low CO_2 increase ($\Delta[CO_2] \sim 20$ ppm) in regions where vegetation productivity is not strongly constrained by climatic conditions, that is, water- or temperature-limited plant growth. Carbon assimilation and carbon pools show stronger responses to eCO_2 across sites while we do not find a widespread strong eCO_2 effect in variables describing the water cycle. The transpiration at canopy level is regulated by the reduced stomatal conductance and meanwhile, the increasing LAI in response to eCO_2. These two opposing effects appear to be cancelled each other out at ecosystem level and longer time scales, resulting in an insignificant eCO_2 effect on transpiration and other water cycle variables (e.g., evaporation, interception loss and soil moisture) which are affected by the response of Tr. While mostly GPP and LAI are the first variables to exhibit detectable eCO_2 effects, in northern high-latitude regions where vegetation growth is limited by radiation, LUE responds to eCO_2 first among all the other variables, and the eCO_2 effects on WUE emerges first in some sites located in semi-arid regions.

Climate variations can partly explain the spatial heterogeneity of the plant physiological effects of eCO_2. The strongest response of GPP or Tr_{norm} to eCO_2 occurs dominantly where GPP is not limited by either temperature or precipitation (e.g., sites in tropical regions). The weakest response of GPP or Tr_{norm} occurs in arid regions (e.g., grassland sites), where the high variability overshadows the eCO_2 effect. In addition to climate factors, eCO_2-induced plant physiological effects are amplified where vegetation productivity is already high. We find the long-term mean LAI is the dominant driver of spatial variability of the eCO_2 effect on GPP, whereas the long-term mean GPP is the dominant driver of spatial variability of the eCO_2 effect on Tr_{norm}. Despite the different model structures and simulation setups, the CMIP6 models essentially are consistent with the insights gained from the QUINCY model about what drives spatial variance in the EoC. Overall, our results thus suggest that high-LAI regions, for example, tree-dominated ecosystems are more sensitive to the eCO_2 effect than low-LAI, for example, grass-dominated ecosystems.

Models have the advantage for hypothesis testing by conducting idealized experiments. Using these experiments, we determine when and where we expect to detect the eCO_2 effects according to our theoretical understanding formulated in the models. This knowledge provides a first step toward assessing long-term changes and trends in carbon and water flux observations using eddy covariance measurements (Baldocchi et al., 2001). In a future study, we will apply this methodology to analyze whether eCO_2 effects can already be detected in the time series of long-term measurement campaigns of land–atmosphere exchange fluxes, focusing on the regions and time scales of eCO_2 effects spotlighted in this precursory study. Overall, the model-based analyses presented here, along with the ongoing observational study focused on the detection and potential quantification of eCO_2 effects, are critical and have long been called for to provide robust assessments of how the system will continue to change as CO_2 continues to rise.

AUTHOR CONTRIBUTIONS

Chunhui Zhan, Rene Orth, and Alexander J. Winkler jointly designed this study. Mirco Migliavacca, Sönke Zaehle, and Markus Reichstein contributed to ideas and experimental design. Alexander J. Winkler preprocessed the CMIP6 model simulations. Jan Engel contributed to technical assistance for the QUINCY model. All authors contributed to the writing of the paper, the discussion, and interpretation of the results.

ACKNOWLEDGMENTS

Chunhui Zhan is supported by the International Max Planck Research School (IMPRS). Markus Reichstein and Alexander J. Winkler acknowledge the support by the European Research Council (ERC) Synergy Grant "Understanding and Modelling the Earth System with Machine Learning (USMILE)" under the Horizon 2020 research and innovation programme (grant agreement number 855187). René Orth is supported by the German Research Foundation (Emmy Noether grant number 391059971). Sönke Zaehle and Jan Engel were supported by the European Research Council (ERC) under the European Union's Horizon 2020 research and innovation programme (QUINCY; grant number 647204). Chunhui Zhan thanks Silvia Caldararu and Lin Yu for their support in working with the QUINCY model. Open Access funding enabled and organized by Projekt DEAL.

FUNDING STATEMENT

Open Access funding enabled and organized by Projekt DEAL

CONFLICT OF INTEREST

The authors declare that there are no competing interests.

DATA AVAILABILITY STATEMENT

The data that support the findings of this study are openly available under https://doi.org/10.5061/dryad.3xsj3txk5.

ORCID

Chunhui Zhan https://orcid.org/0000-0001-7716-8969
Sönke Zaehle https://orcid.org/0000-0001-5602-7956

REFERENCES

Ainsworth, E. A., & Long, S. P. (2005). What have we learned from 15 years of free-air CO_2 enrichment (FACE)? A meta-analytic review of the responses of photosynthesis, canopy properties and

plant production to rising CO_2. *The New Phytologist*, *165*, 351–372. https://doi.org/10.1111/j.1469-8137.2004.01224.x

Ainsworth, E. A., & Rogers, A. (2007). The response of photosynthesis and stomatal conductance to rising [CO_2]: Mechanisms and environmental interactions. *Plant, Cell and Environment*, *30*, 258–270. https://doi.org/10.1111/j.1365-3040.2007.01641.x

Arora, V. K., Katavouta, A., Williams, R. G., Jones, C. D., Brovkin, V., Friedlingstein, P., Schwinger, J., Bopp, L., Boucher, O., Cadule, P., Chamberlain, M. A., Christian, J. R., Delire, C., Fisher, R. A., Hajima, T., Ilyina, T., Joetzjer, E., Kawamiya, M., Koven, C. D., … Ziehn, T. (2020). Carbon–concentration and carbon–climate feedbacks in CMIP6 models and their comparison to CMIP5 models. *Biogeosciences*, *17*, 4173–4222. https://doi.org/10.5194/bg-17-4173-2020

Baig, S., Medlyn, B. E., Mercado, L. M., & Zaehle, S. (2015). Does the growth response of woody plants to elevated CO_2 increase with temperature? A model-oriented meta-analysis. *Global Change Biology*, *21*, 4303–4319. https://doi.org/10.1111/gcb.12962

Baldocchi, D., Falge, E., Gu, L., Olson, R., Hollinger, D., Running, S., Anthoni, P., Bernhofer, C., Davis, K., Evans, R., Fuentes, J., Goldstein, A., Katul, G., Law, B., Lee, X., Malhi, Y., Meyers, T., Munger, W., Oechel, W., … Wofsy, S. (2001). FLUXNET: A new tool to study the temporal and spatial variability of ecosystem-scale carbon dioxide, water vapor, and energy flux densities. *Bulletin of the American Meteorological Society*, *82*, 2415–2434. https://doi.org/10.1175/1520-0477(2001)082<2415:FANTTS>2.3.CO;2

Barton, C. V. M., Duursma, R. A., Medlyn, B. E., Ellsworth, D. S., Eamus, D., Tissue, D. T., Adams, M. A., Conroy, J., Crous, K. Y., Liberloo, M., Löw, M., Linder, S., & McMurtrie, R. E. (2012). Effects of elevated atmospheric [CO_2] on instantaneous transpiration efficiency at leaf and canopy scales in *Eucalyptus saligna*. *Global Change Biology*, *18*, 585–595. https://doi.org/10.1111/j.1365-2486.2011.02526.x

Bastos, A., Ciais, P., Friedlingstein, P., Sitch, S., Pongratz, J., Fan, L., Wigneron, J. P., Weber, U., Reichstein, M., Fu, Z., Anthoni, P., Arneth, A., Haverd, V., Jain, A. K., Joetzjer, E., Knauer, J., Lienert, S., Loughran, T., McGuire, P. C., … Zaehle, S. (2020). Direct and seasonal legacy effects of the 2018 heat wave and drought on European ecosystem productivity. *Science Advances*, *6*(24), eaba2724. https://doi.org/10.1126/sciadv.aba2724

Chen, J. M., Mo, G., Pisek, J., Liu, J., Deng, F., Ishizawa, M., & Chan, D. (2012). Effects of foliage clumping on the estimation of global terrestrial gross primary productivity. *Global Biogeochemical Cycles*, *26*, GB1019. https://doi.org/10.1029/2010GB003996

Cleveland, W. S. (1981). LOWESS: A program for smoothing scatterplots by robust locally weighted regression. *The American Statistician*, *35*, 54 10.2307/2683591De

De Kauwe, M. G., Medlyn, B. E., Knauer, J., & Williams, C. A. (2017). Ideas and perspectives: How coupled is the vegetation to the boundary layer? *Biogeosciences*, *14*, 4435–4453 10.5194/bg-14-4435-2017

De Kauwe, M. G., Medlyn, B. E., & Tissue, D. T. (2021). To what extent can rising [CO_2] ameliorate plant drought stress? *The New Phytologist*, *231*, 2118–2124. https://doi.org/10.1111/nph.17540

De Kauwe, M. G., Medlyn, B. E., Zaehle, S., Walker, A. P., Dietze, M. C., Wang, Y.-P., Luo, Y., Jain, A. K., El-Masri, B., Hickler, T., Wårlind, D., Weng, E., Parton, W. J., Thornton, P. E., Wang, S., Prentice, I. C., Asao, S., Smith, B., McCarthy, H. R., … Norby, R. J. (2014). Where does the carbon go? A model–data intercomparison of vegetation carbon allocation and turnover processes at two temperate forest free-air CO_2 enrichment sites. *The New Phytologist*, *203*, 883–899. https://doi.org/10.1111/nph.12847

Denissen, J. M. C., Teuling, A. J., Pitman, A. J., Koirala, S., Migliavacca, M., Li, W., Reichstein, M., Winkler, A. J., Zhan, C., & Orth, R. (2022). Widespread shift from ecosystem energy to water limitation with climate change. *Nature Climate Change*, *12*, 677–684. https://doi.org/10.1038/s41558-022-01403-8

Drake, B. G., Gonzàlez-Meler, M. A., & Long, S. P. (1997). More efficient plants: A consequence of rising atmospheric CO_2? *Annual Review of Plant Physiology and Plant Molecular Biology*, *48*, 609–639. https://doi.org/10.1146/annurev.arplant.48.1.609

Fernández-Martínez, M., Vicca, S., Janssens, I. A., Ciais, P., Obersteiner, M., Bartrons, M., Sardans, J., Verger, A., Canadell, J. G., Chevallier, F., Wang, X., Bernhofer, C., Curtis, P. S., Gianelle, D., Grünwald, T., Heinesch, B., Ibrom, A., Knohl, A., Laurila, T., … Peñuelas, J. (2017). Atmospheric deposition, CO_2, and change in the land carbon sink. *Scientific Reports*, *7*, 9632. https://doi.org/10.1038/s41598-017-08755-8

Friedlingstein, P., Jones, M. W., O'Sullivan, M., Andrew, R. M., Hauck, J., Peters, G. P., Peters, W., Pongratz, J., Sitch, S., Le Quéré, C., Bakker, D. C. E., Canadell, J. G., Ciais, P., Jackson, R. B., Anthoni, P., Barbero, L., Bastos, A., Bastrikov, V., Becker, M., … Zaehle, S. (2019). Global carbon budget 2019. *Earth System Science Data*, *11*, 1783–1838. https://doi.org/10.5194/essd-11-1783-2019

Gedney, N., Cox, P. M., Betts, R. A., Boucher, O., Huntingford, C., & Stott, P. A. (2006). Detection of a direct carbon dioxide effect in continental river runoff records. *Nature*, *439*, 835–838. https://doi.org/10.1038/nature04504

Good, S. P., Noone, D., & Bowen, G. (2015). Hydrologic connectivity constrains partitioning of global terrestrial water fluxes. *Science*, *349*, 175–177. https://doi.org/10.1126/science.aaa5931

Harris, I., Osborn, T. J., Jones, P., & Lister, D. (2020). Version 4 of the CRU TS monthly high-resolution gridded multivariate climate dataset. *Scientific Data*, *7*, 109. https://doi.org/10.1038/s41597-020-0453-3

Hengl, T., de Jesus, J. M., Heuvelink, G. B. M., Gonzalez, M. R., Kilibarda, M., Blagotić, A., Shangguan, W., Wright, M. N., Geng, X., Bauer-Marschallinger, B., Guevara, M. A., Vargas, R., MacMillan, R. A., Batjes, N. H., Leenaars, J. G. B., Ribeiro, E., Wheeler, I., Mantel, S., & Kempen, B. (2017). SoilGrids250m: Global gridded soil information based on machine learning. *PLoS ONE*, *12*, e0169748. https://doi.org/10.1371/journal.pone.0169748

Hickler, T., Smith, B., Prentice, I. C., Mjöfors, K., Miller, P., Arneth, A., & Sykes, M. T. (2008). CO_2 fertilization in temperate FACE experiments not representative of boreal and tropical forests. *Global Change Biology*, *14*, 1531–1542. https://doi.org/10.1111/j.1365-2486.2008.01598.x

Jarvis, P. G. (1985). Transpiration and assimilation of tree and agricultural crops: The 'omega factor'. In M. G. R. Cannell & J. E. Jackson (Eds.), *Attributes of trees as crop plants* (pp. 460–480). Institute of Terrestrial Ecology.

Jones, C. D., Arora, V., Friedlingstein, P., Bopp, L., Brovkin, V., Dunne, J., Graven, H., Hoffman, F., Ilyina, T., John, J. G., Jung, M., Kawamiya, M., Koven, C., Pongratz, J., Raddatz, T., Randerson, J. T., & Zaehle, S. (2016). C4MIP – The Coupled Climate–Carbon Cycle Model Intercomparison Project: experimental protocol for CMIP6. *Geoscientific Model Development*, *9*, 2853–2880. https://doi.org/10.5194/gmd-9-2853-2016

Keenan, T. F., Hollinger, D. Y., Bohrer, G., Dragoni, D., Munger, J. W., Schmid, H. P., & Richardson, A. D. (2013). Increase in forest water-use efficiency as atmospheric carbon dioxide concentrations rise. *Nature*, *499*, 324–327. https://doi.org/10.1038/nature12291

Knauer, J., Zaehle, S., Reichstein, M., Medlyn, B. E., Forkel, M., Hagemann, S., & Werner, C. (2017). The response of ecosystem water-use efficiency to rising atmospheric CO_2 concentrations: Sensitivity and large-scale biogeochemical implications. *The New Phytologist*, *213*, 1654–1666. https://doi.org/10.1111/nph.14288

Konings, A. G., Williams, A. P., & Gentine, P. (2017). Sensitivity of grassland productivity to aridity controlled by stomatal and xylem regulation. *Nature Geoscience*, *10*, 284–288. https://doi.org/10.1038/ngeo2903

Körner, C., Morgan, J., & Norby, R. (2007). CO_2 fertilization: When, where, how much? In J. G. Canadell, D. E. Pataki, & L. F. Pitelka (Eds.), *Terrestrial ecosystems in a changing world, global change—The IGBP series* (pp. 9–21). Springer. https://doi.org/10.1007/978-3-540-32730-1_2

Kramer, P. J. (1981). Carbon dioxide concentration, photosynthesis, and dry matter production. *Bioscience*, *31*, 29–33. https://doi.org/10.2307/1308175

Kull, O., & Kruijt, B. (1998). Leaf photosynthetic light response: A mechanistic model for scaling photosynthesis to leaves and canopies. *Functional Ecology*, *12*, 767–777. https://doi.org/10.1046/j.1365-2435.1998.00257.x

Kulmatiski, A., Adler, P. B., & Foley, K. M. (2020). Hydrologic niches explain species coexistence and abundance in a shrub–steppe system. *Journal of Ecology*, *108*, 998–1008. https://doi.org/10.1111/1365-2745.13324

Le Quéré, C., Andrew, R. M., Friedlingstein, P., Sitch, S., Pongratz, J., Manning, A. C., Korsbakken, J. I., Peters, G. P., Canadell, J. G., Jackson, R. B., Boden, T. A., Tans, P. P., Andrews, O. D., Arora, V. K., Bakker, D. C. E., Barbero, L., Becker, M., Betts, R. A., Bopp, L., … Zhu, D. (2018). Global carbon budget 2017. *Earth System Science Data*, *10*, 405–448. https://doi.org/10.5194/essd-10-405-2018

Leakey, A. D. B., Ainsworth, E. A., Bernacchi, C. J., Rogers, A., Long, S. P., & Ort, D. R. (2009). Elevated CO_2 effects on plant carbon, nitrogen, and water relations: Six important lessons from FACE. *Journal of Experimental Botany*, *60*, 2859–2876. https://doi.org/10.1093/jxb/erp096

Lee, H., Park, J., Cho, S., Lee, M., & Kim, H. S. (2019). Impact of leaf area index from various sources on estimating gross primary production in temperate forests using the JULES land surface model. *Agricultural and Forest Meteorology*, *276–277*, 107614. https://doi.org/10.1016/j.agrformet.2019.107614

Lemordant, L., Gentine, P., Swann, A. S., Cook, B. I., & Scheff, J. (2018). Critical impact of vegetation physiology on the continental hydrologic cycle in response to increasing CO_2. *Proceedings of the National Academy of Sciences of the United States of America*, *115*, 4093–4098. https://doi.org/10.1073/pnas.1720712115

Leuzinger, S., & Körner, C. (2007). Water savings in mature deciduous forest trees under elevated CO_2. *Global Change Biology*, *13*, 2498–2508. https://doi.org/10.1111/j.1365-2486.2007.01467.x

Liu, J., You, Y., Li, J., Sitch, S., Gu, X., Nabel, J. E. M. S., Lombardozzi, D., Luo, M., Feng, X., Arneth, A., Jain, A. K., Friedlingstein, P., Tian, H., Poulter, B., & Kong, D. (2021). Response of global land evapotranspiration to climate change, elevated CO_2, and land use change. *Agricultural and Forest Meteorology*, *311*, 108663. https://doi.org/10.1016/j.agrformet.2021.108663

Long, S. P. (1991). Modification of the response of photosynthetic productivity to rising temperature by atmospheric CO_2 concentrations: Has its importance been underestimated? *Plant, Cell and Environment*, *14*, 729–739. https://doi.org/10.1111/j.1365-3040.1991.tb01439.x

Lundberg, S., & Lee, S.-I. (2017). A unified approach to interpreting model predictions. *Advances in Neural Information Processing Systems*, 4765–4774.

Lundberg, S. M., Erion, G., Chen, H., DeGrave, A., Prutkin, J. M., Nair, B., Katz, R., Himmelfarb, J., Bansal, N., & Lee, S.-I. (2020). From local explanations to global understanding with explainable AI for trees. *Nature Machine Intelligence*, *2*, 56–67. https://doi.org/10.1038/s42256-019-0138-9

Maurer, G. E., Hallmark, A. J., Brown, R. F., Sala, O. E., & Collins, S. L. (2020). Sensitivity of primary production to precipitation across the United States. *Ecology Letters*, *23*, 527–536. https://doi.org/10.1111/ele.13455

McCarthy, H. R., Oren, R., Finzi, A. C., & Johnsen, K. H. (2006). Canopy leaf area constrains $[CO_2]$-induced enhancement of productivity and partitioning among aboveground carbon pools. *Proceedings of the National Academy of Sciences of the United States of America*, *103*, 19356–19361. https://doi.org/10.1073/pnas.0609448103

McCarthy, H. R., Oren, R., Johnsen, K. H., Gallet-Budynek, A., Pritchard, S. G., Cook, C. W., LaDeau, S. L., Jackson, R. B., & Finzi, A. C. (2010). Re-assessment of plant carbon dynamics at the Duke free-air CO_2 enrichment site: Interactions of atmospheric $[CO_2]$ with nitrogen and water availability over stand development. *The New Phytologist*, *185*, 514–528. https://doi.org/10.1111/j.1469-8137.2009.03078.x

Medlyn, B. E., Barton, C. V. M., Broadmeadow, M. S. J., Ceulemans, R., De Angelis, P., Forstreuter, M., Freeman, M., Jackson, S. B., Kellomäki, S., Laitat, E., Rey, A., Roberntz, P., Sigurdsson, B. D., Strassemeyer, J., Wang, K., Curtis, P. S., & Jarvis, P. G. (2001). Stomatal conductance of forest species after long-term exposure to elevated CO_2 concentration: A synthesis. *The New Phytologist*, *149*, 247–264. https://doi.org/10.1046/j.1469-8137.2001.00028.x

Medlyn, B. E., Duursma, R. A., Eamus, D., Ellsworth, D. S., Prentice, I. C., Barton, C. V. M., Crous, K. Y., Angelis, P. D., Freeman, M., & Wingate, L. (2011). Reconciling the optimal and empirical approaches to modelling stomatal conductance. *Global Change Biology*, *17*, 2134–2144. https://doi.org/10.1111/j.1365-2486.2010.02375.x

Meehl, G. A., Moss, R., Taylor, K. E., Eyring, V., Stouffer, R. J., Bony, S., & Stevens, B. (2014). Climate model intercomparisons: Preparing for the next phase. *EOS. Transactions of the American Geophysical Union*, *95*, 77–78. https://doi.org/10.1002/2014EO090001

Migliavacca, M., Musavi, T., Mahecha, M. D., Nelson, J. A., Knauer, J., Baldocchi, D. D., Perez-Priego, O., Christiansen, R., Peters, J., Anderson, K., Bahn, M., Black, T. A., Blanken, P. D., Bonal, D., Buchmann, N., Caldararu, S., Carrara, A., Carvalhais, N., Cescatti, A., … Reichstein, M. (2021). The three major axes of terrestrial ecosystem function. *Nature*, *598*, 468–472. https://doi.org/10.1038/s41586-021-03939-9

Miguez-Macho, G., & Fan, Y. (2021). Spatiotemporal origin of soil water taken up by vegetation. *Nature*, *598*, 624–628. https://doi.org/10.1038/s41586-021-03958-6

Norby, R. J., DeLucia, E. H., Gielen, B., Calfapietra, C., Giardina, C. P., King, J. S., Ledford, J., McCarthy, H. R., Moore, D. J. P., Ceulemans, R., Angelis, P. D., Finzi, A. C., Karnosky, D. F., Kubiske, M. E., Lukac, M., Pregitzer, K. S., Scarascia-Mugnozza, G. E., Schlesinger, W. H., & Oren, R. (2005). Forest response to elevated CO_2 is conserved across a broad range of productivity. *Proceedings of the National Academy of Sciences of the United States of America*, *102*, 18052–18056. https://doi.org/10.1073/pnas.0509478102

Norby, R. J., Wullschleger, S. D., Gunderson, C. A., Johnson, D. W., & Ceulemans, R. (1999). Tree responses to rising CO_2 in field experiments: Implications for the future forest. *Plant, Cell and Environment*, *22*, 683–714. https://doi.org/10.1046/j.1365-3040.1999.00391.x

Norby, R. J., & Zak, D. R. (2011). Ecological lessons from free-air CO_2 enrichment (FACE) experiments. *Annual Review of Ecology, Evolution, and Systematics*, *42*, 181–203. https://doi.org/10.1146/annurev-ecolsys-102209-144647

Novick, K. A., Ficklin, D. L., Stoy, P. C., Williams, C. A., Bohrer, G., Oishi, A. C., Papuga, S. A., Blanken, P. D., Noormets, A., Sulman, B. N., Scott, R. L., Wang, L., & Phillips, R. P. (2016). The increasing importance of atmospheric demand for ecosystem water and carbon fluxes. *Nature Climate Change*, *6*, 1023–1027. https://doi.org/10.1038/nclimate3114

Pedregosa, F., Varoquaux, G., Gramfort, A., Michel, V., Thirion, B., Grisel, O., Blondel, M., Prettenhofer, P., Weiss, R., Dubourg, V., Vanderplas, J., Passos, A., & Cournapeau, D. (2011). Scikit-learn: Machine learning in Python, *6*.

Peñuelas, J., Canadell, J. G., & Ogaya, R. (2011). Increased water-use efficiency during the 20th century did not translate into enhanced tree growth. *Global Ecology and Biogeography*, *20*, 597–608. https://doi.org/10.1111/j.1466-8238.2010.00608.x

Reichstein, M., Bahn, M., Ciais, P., Frank, D., Mahecha, M. D., Seneviratne, S. I., Zscheischler, J., Beer, C., Buchmann, N., Frank, D. C., Papale, D., Rammig, A., Smith, P., Thonicke, K., van der Velde, M., Vicca, S., Walz, A., & Wattenbach, M. (2013). Climate extremes and the carbon cycle. *Nature*, *500*, 287–295. https://doi.org/10.1038/nature12350

Saxton, K. E., & Rawls, W. J. (2006). Soil water characteristic estimates by texture and organic matter for hydrologic solutions. *Soil Science*

Society of America Journal, *70*, 1569–1578. https://doi.org/10.2136/sssaj2005.0117

Schimel, D., Stephens, B. B., & Fisher, J. B. (2015). Effect of increasing CO_2 on the terrestrial carbon cycle. *Proceedings of the National Academy of Sciences of the United States of America*, *112*, 436–441. https://doi.org/10.1073/pnas.1407302112

Street, L. E., Shaver, G. R., Williams, M., & Van Wijk, M. T. (2007). What is the relationship between changes in canopy leaf area and changes in photosynthetic CO_2 flux in arctic ecosystems? *Journal of Ecology*, *95*, 139–150 10.1111/j.1365-2745.2006.01187.x

Thum, T., Caldararu, S., Engel, J., Kern, M., Pallandt, M., Schnur, R., Yu, L., & Zaehle, S. (2019). A new model of the coupled carbon, nitrogen, and phosphorus cycles in the terrestrial biosphere (QUINCY v1.0; revision 1996). *Geoscientific Model Development*, *12*, 4781–4802 10.5194/gmd-12-4781-2019

Ueyama, M., Ichii, K., Kobayashi, H., Kumagai, T., Beringer, J., Merbold, L., Euskirchen, E. S., Hirano, T., Marchesini, L. B., Baldocchi, D., Saitoh, T. M., Mizoguchi, Y., Ono, K., Kim, J., Varlagin, A., Kang, M., Shimizu, T., Kosugi, Y., Bret-Harte, M. S., … Yasuda, Y. (2020). Inferring CO_2 fertilization effect based on global monitoring land-atmosphere exchange with a theoretical model. *Environmental Research Letters*, *15*, 084009. https://doi.org/10.1088/1748-9326/ab79e5

van der Sleen, P., Groenendijk, P., Vlam, M., Anten, N. P. R., Boom, A., Bongers, F., Pons, T. L., Terburg, G., & Zuidema, P. A. (2015). No growth stimulation of tropical trees by 150 years of CO_2 fertilization but water-use efficiency increased. *Nature Geoscience*, *8*, 24–28. https://doi.org/10.1038/ngeo2313

Walker, A. P., De Kauwe, M. G., Bastos, A., Belmecheri, S., Georgiou, K., Keeling, R. F., McMahon, S. M., Medlyn, B. E., Moore, D. J. P., Norby, R. J., Zaehle, S., Anderson-Teixeira, K. J., Battipaglia, G., Brienen, R. J. W., Cabugao, K. G., Cailleret, M., Campbell, E., Canadell, J. G., Ciais, P., … Zuidema, P. A. (2021). Integrating the evidence for a terrestrial carbon sink caused by increasing atmospheric CO_2. *The New Phytologist*, *229*, 2413–2445. https://doi.org/10.1111/nph.16866

Walker, A. P., De Kauwe, M. G., Medlyn, B. E., Zaehle, S., Iversen, C. M., Asao, S., Guenet, B., Harper, A., Hickler, T., Hungate, B. A., Jain, A. K., Luo, Y., Lu, X., Lu, M., Luus, K., Megonigal, J. P., Oren, R., Ryan, E., Shu, S., … Norby, R. J. (2019). Decadal biomass increment in early secondary succession woody ecosystems is increased by CO_2 enrichment. *Nature Communications*, *10*, 454. https://doi.org/10.1038/s41467-019-08348-1

Way, D. A., Katul, G. G., Manzoni, S., & Vico, G. (2014). Increasing water use efficiency along the C3 to C4 evolutionary pathway: A stomatal optimization perspective. *Journal of Experimental Botany*, *65*, 3683–3693. https://doi.org/10.1093/jxb/eru205

Weisstein, E. W. (n.d.). "Least Squares Fitting" from MathWorld–A Wolfram web resource. https://mathworld.wolfram.com/LeastSquaresFitting.html

Williams, I. N., & Torn, M. S. (2015). Vegetation controls on surface heat flux partitioning, and land-atmosphere coupling. *Geophysical Research Letters*, *42*, 9416–9424. https://doi.org/10.1002/2015GL066305

Winkler, A. J., Myneni, R. B., Hannart, A., Sitch, S., Haverd, V., Lombardozzi, D., Arora, V. K., Pongratz, J., Nabel, J. E. M. S., Goll, D. S., Kato, E., Tian, H., Arneth, A., Friedlingstein, P., Jain, A. K., Zaehle, S., & Brovkin, V. (2021). Slowdown of the greening trend in natural vegetation with further rise in atmospheric CO_2. *Biogeosciences*, *18*, 4985–5010. https://doi.org/10.5194/bg-18-4985-2021

Woodward, F. I., & Kelly, C. K. (1995). The influence of CO_2 concentration on stomatal density. *The New Phytologist*, *131*, 311–327. https://doi.org/10.1111/j.1469-8137.1995.tb03067.x

Wullschleger, S. D., Tschaplinski, T. J., & Norby, R. J. (2002). Plant water relations at elevated CO_2– implications for water-limited environments. *Plant, Cell and Environment*, *25*, 319–331. https://doi.org/10.1046/j.1365-3040.2002.00796.x

Zaehle, S., & Friend, A. D. (2010). Carbon and nitrogen cycle dynamics in the O-CN land surface model: 1. Model description, site-scale evaluation, and sensitivity to parameter estimates. *Global Biogeochemical Cycles*, *24*, GB1005. https://doi.org/10.1029/2009GB003521

SUPPORTING INFORMATION

Additional supporting information can be found online in the Supporting Information section at the end of this article.

How to cite this article: Zhan, C., Orth, R., Migliavacca, M., Zaehle, S., Reichstein, M., Engel, J., Rammig, A., & Winkler, A. J. (2022). Emergence of the physiological effects of elevated CO_2 on land–atmosphere exchange of carbon and water. *Global Change Biology*, *28*, 7313–7326. https://doi.org/10.1111/gcb.16397